https://doi.org/10.5194/acp-2019-584
Preprint. Discussion started: 7 August 2019

Atmospheric Chemistry and Physics Discussions

Molecular compositions and optical properties of dissolved brown carbon in smoke particles illuminated by excitation-emission matrix spectroscopy and Fourier-transform ion cyclotron resonance mass spectrometry (FT-ICR MS) analysis

Jiao Tang[1,4], Jun Li[*,1], Tao Su[1,4], Yong Han[2], Yangzhi Mo[1], Hongxing, Jiang[1,4], Min Cui[2], Bin Jiang[1], Yingjun Chen[2], Jianhui Tang[3], Jianzhong Song[1], Ping'an Peng[1], Gan Zhang[*,1]

[1]State Key Laboratory of Organic Geochemistry, Guangzhou Institute of Geochemistry, Chinese Academy of Sciences, Guangzhou 510640, China

[2]Department of Environmental Science and Engineering, Fudan University, Shanghai 200092, P.R. China

[3]Key Laboratory of Coastal Environmental Processes and Ecological Remediation, Yantai Institute of Coastal Zone Research, Chinese Academy of Sciences, Yantai 264003, China

[4]University of Chinese Academy of Sciences, Beijing 100049, China

*Corresponding authors: Jun Li (junli@gig.ac.cn); Gan Zhang (zhanggan@gig.ac.cn)

https://doi.org/10.5194/acp-2019-584
Preprint. Discussion started: 7 August 2019

Atmospheric Chemistry and Physics Discussions

Abstract: We investigated the fluorescence and chemical-structural characteristics of dissolved brown carbon (BrC) in smoke particulates emitted from the combustion of biomass and fossil fuels (coal and vehicle exhaust) by excitation-emission matrix (EEM) spectroscopy and Fourier-transform ion cyclotron resonance mass spectrometry (FT-ICR MS) coupled with electrospray ionization (ESI). Six components were resolved by parallel factor analysis (PARAFAC) of the water-soluble and methanol-soluble organic carbon (MSOC) fractions, respectively. These fluorescent components varied among sources. Combined with FT-ICR MS ion groups, we found that the fluorescent components agreed well with the functional groups, particularly with nitrogen (N)- and sulfur (S)-containing groups. Among the six PARAFAC components (P1–6) retrieved from the water-soluble organic carbon (WSOC) fraction, except for the P3 component, the other components exhibited different values among the three types of emission sources tested. Vehicle exhaust was characterized by high P1 and P6 components, which are mainly associated with aromatic organosulfate compounds, and a high P5 component, mainly associated with sulfonates; coal combustion was characterized by a high P4 component, which is associated with nitrooxy-organosulfate (nitrooxy-OS) compounds; and biomass burning was characterized by the P2 component. Similar results were observed in the case of the MSOC fraction. This study reveals the source contribution and possible structures of previously unclear excitation-emission matrix (EEM) fluorescent components in combustion-derived aerosols. These are the first findings of this type and are potentially applicable to further studies on EEM-based source apportionment of dissolved BrC in aerosols.

https://doi.org/10.5194/acp-2019-584
Preprint. Discussion started: 7 August 2019

Atmospheric Chemistry and Physics Discussions

1 Introduction

Carbonaceous aerosols play an important role in the Earth's radiative balance. One such aerosol, black carbon (BC), absorbs significant amounts of light and exerts a warming effect, while organic carbon (OC) was initially thought to only scatter solar radiation (Wong et al., 2017;Mo et al., 2017;Saleh et al., 2014). However, there are certain types of OC that absorb radiation efficiently in the near ultraviolet (UV) (300–400 nm) and UV-visible (UV-Vis) ranges, which are called brown carbon (BrC) and are able to positively shift the net direct radiation forcing (DRF) (Saleh et al., 2014;Laskin et al., 2015;Chen and Bond, 2009;Kirchstetter and Thatcher, 2012). According to a simulation model, the inclusion of BrC may enhance total aerosol absorption by 7–19% (Feng et al., 2013). BrC mainly originates from emissions from biomass burning and fossil fuel combustion, and the formation of secondary organic aerosol (SOA) (Zhu et al., 2018;Laskin et al., 2015). Among the various sources listed above, primary emissions contributed significantly to BrC absorption (Fan et al., 2012;Yan et al., 2015;Zhang et al., 2011). Recently, many studies have investigated the chemical and optical properties of BrC in smoke particles emitted from biomass burning, coal combustion in a control laboratory chamber (Park and Yu, 2016;Fan et al., 2016;Chen and Bond, 2009) and emissions characteristic of vehicle emissions (Dai et al., 2015). However, most studies mainly focused on light absorption of BrC; little structural information is available.

Excitation-emission matrix (EEM) spectroscopy has been widely applied to identify the sources and chemical nature of chromophoric dissolved organic matter (CDOM) in aquatic environments since the 1990s (Shimabuku et al., 2017;Wells et al., 2017;Bhattacharya and Osburn, 2017;Coble, 1996), while few studies have focused on the fluorescence properties of chromophores in atmospheric environments. Recently, many studies have suggested that the optical properties of chromophoric water-soluble organic carbon (WSOC) in the atmosphere was similar to CDOM in aquatic environments (Qin et al., 2018;Fu et al., 2015), and this could be extended to atmospheric research. Fluorescence is a radiative process that occurs between two

https://doi.org/10.5194/acp-2019-584
Preprint. Discussion started: 7 August 2019


Atmospheric Chemistry and Physics Discussions

energy levels of the same multiplicity (Andrade-Eiroa et al., 2013). Compounds with rigid planar structures and highly conjugated systems have intrinsic fluorescence emission characteristics, such as aromatic acids, phenols, nitroaromatics, polycyclic aromatic hydrocarbons (PAHs), quinones, and so on, which are important BrC chromophores (Lin et al., 2018;Zhang et al., 2013). Furthermore, Laskin et al.(Laskin et al., 2015) believed that fluorescence is sensitive to the molecular (or supramolecular) identity of BrC compounds and anticipated that fluorescence-based methods will become increasingly important in the study of BrC. Fluorescence spectra, which are considered a "fingerprinting" tool, have been applied to organic aerosols (Fu et al., 2015;Chen et al., 2016b). Chen et al.(Chen et al., 2016b) observed that the fluorescence spectra of water-soluble organic matter from urban, forest, and marine aerosols varied depending on the sampling site and period, and were affected by oxidative and functional groups. Lee et al.(Lee et al., 2013) reported that SOA derived from the oxidation of limonene and decene with O_3 and OH presented different fluorescence spectra. The biggest challenge when analyzing chromophoric BrC using fluorescence spectra, however, is the lack of a classification system for fluorescence spectra, to distinguish chromophores from the majority of nonabsorbing constituents and to determine the chemical structures of the chromophores. The combination of Fourier-transform ion cyclotron resonance mass spectrometry (FT-ICR MS) coupled with electrospray ionization (ESI) and EEM is a powerful platform for characterizing BrC chromophores, and is expected to enable us to deduce the molecular compositions of these chromophores. FT-ICR MS has been successfully used to characterize organic aerosol (Jiang et al., 2016;Song et al., 2018;Mo et al., 2018), cloud water (Zhao et al., 2013), and natural organic matter (Sleighter et al., 2012;Feng et al., 2016). The ultrahigh resolution, accuracy of mass measurements, and high sensitivity make this technique suitable for studying complex mixtures at the molecular level, and for identifying the chemical compositions of the substances being studied with a high degree of confidence (Feng et al., 2016).

Residential coal combustion and biomass burning are very important anthropogenic sources of air pollutants, especially fine particulate matter ($PM_{2.5}$), in

https://doi.org/10.5194/acp-2019-584
Preprint. Discussion started: 7 August 2019

Atmospheric Chemistry and Physics Discussions

China (Tian et al., 2017). Concerns about the environmental and health effects of vehicle emissions have existed for decades (Dai et al., 2015). The characteristics of BrC from these origins may differ to those of BrC from other sources. To obtain a comprehensive understanding of BrC originating from different sources, we investigated the solvent extractions of organic compounds with different polarities from the smoke particles of simulated combustion emissions from biomass fuel, coal, and vehicles, and characterized their optical properties in terms of UV-Vis absorption and excitation-emission matrix (EEM) spectra. We employed FT-ICR MS coupled with ESI to investigate the molecular compositions of the fluorescent components identified by parallel factor analysis (PARAFAC). We also aimed to identify the possible chemical structures of these chromophores and create a source library of BrC chromophores for applications to atmospheric BrC apportionment based on fluorescence technology.

2 Experimental methods

2.1 Sample collection and preparation

The smoke particle were collected by the instrument coupled with dilution channel which was designed to simulate fire emissions representative of "real-world" open biomass burning and household coal combustion activities (Figure S1). In present study, a total of 27 biomass burning samples (IDs: 1-27) were collected at Xishuangbanna city, Yunnan Provence, from May 20th to June 3th, 2016 and the detailed sampling process was described in our previous article (Cui et al., 2018). In short, raw fuels (rough 20×3×2 cm^3) were air-dried for several days, and ignited in a stainless steel bowl, and then the rising smoke was collected through a dilution system. The sampling system mainly consisted of a dilution tunnel, a residence time chamber, three particulate matter (PM) samplers, and so on. Every biomass about 1-2 kg fuels was burned three times, and each combustion process lasted for 20 minutes. The collection of smoke particle started when fuel ignited, and end until the concentration of CO_2 down to atmosphere CO_2 level. Dilution ratios of each experimental process

https://doi.org/10.5194/acp-2019-584
Preprint. Discussion started: 7 August 2019


Atmospheric Chemistry and Physics Discussions

were calculated using the CO_2 concentrations before and after dilution. The collection flow rate and average dilution ratio were 180 L/min and 2.1, respectively. And the other 6 biomass burning samples (IDs: 28-33) were collected at Guangzhou city, Guangdong Province.

The smoke particle of coal combustion (IDs: 34-50) were collected as same as that of biomass burning, but used a stove, at Guangzhou city, Guangdong province, from Nov 18th, 2017 to Jan 23th, 2018. The tested stove is technically improved stoves (named Jin-Yin stove). Due to the difficult of ignition of coal, we used smokeless charcoal to ignite one-third (about 300 g) of the raw-coal chunk (2-5 cm in size) in stove, removed the charcoal after ignition, and then added the remaining raw-coal chunk (about 700 g) to start to collect the smoke particle. Every coal about 1 kg fuels was burned three times, and each combustion process lasted for about 40-150 minutes. The collection flow rate and average dilution ratio were 150 L/min and 1.5, respectively. Additional, a modified combustion efficiency (MCE) was calculated to characterize the relative amount of smoldering and flaming combustion phase (Lin et al., 2016;Cui et al., 2018). The average MCE values were 0.73 ± 0.08 for coal combustion, but unavailable for biomass burning because the CO sensor did not work in the field work which was mentioned in our previous paper (Cui et al., 2018).

Eight tunnel samples (IDs: 51-58) were collected at Siping Tunnel from Nov 1th to 2th, 2017 and Xiaoyangshan Tunnel from Dec 1th to 2 th, 2017, in Shanghai city, as well as two vehicle exhaust samples (IDs: 59-60) were collected from truck. The filters were wrapped in aluminum foil and pre-baked at 450 °C for 5 hours before sampling, and stored at -20 °C after sampling. There were a total of 60 total suspended particulate matter (TSP) samples on source emission in the current experiment, and blank samples which were collected at different times and locations were used for correcting filter samples.

WSOC for UV-Vis absorption and EEM analysis was extracted with purified water (resistivity of >18.2Ω) via ultra-sonication of quartz filter punches for 30 minutes. After the extraction, we obtained the methanol-soluble organic carbon (MSOC) constituent by freeze drying the water-extracted filter and performing

https://doi.org/10.5194/acp-2019-584
Preprint. Discussion started: 7 August 2019


Atmospheric Chemistry and Physics Discussions

ultrasonic-extraction with methanol (HPLC grade) in the same manner. Note that the MSOC fraction of the methanol extract in our current study are not necessarily similar to those of the same names in other studies. All of the extracts were filtered through a 0.22 um polytetrafluoroethylene membrane into amber colored glass vials to remove the insoluble material.

2.2 Carbon analysis

We measured both OC and elemental carbon (EC) using an aerosol carbon analyzer (Sunset Laboratory, Inc., USA), following the NIOSH thermal-optical transmittance (TOT) standard method (Mo et al., 2017), and the emission factors (EFs) of PM, OC and EC were calculated and detail information was presented in supplement. We also analyzed the elemental compositions of biomass (C, H, O, and N) and coal (C, H, O, N, and S) using an elemental analyzer (vario EL cube; Elementar, Germany) and the results were listed in Table S1 and S2. The carbon content of WSOC were measured using total organic carbon analysis (Vario TOC cube; Elementar) before acidifying with phosphoric acid to remove inorganic carbon, while that of the MSOC fractions were assessed using the method developed by Chen et al (Chen et al., 2017b). In short, the extracted MSOC fraction was dried gently under nitrogen, and then re-dissolved in 500 μL methanol. Subsequently, 50 μL of the solution was added to the clear quartz filter (area: 1.5 cm^2) until dry, and analyzed using the TOT standard method.

2.3 UV−Vis absorption spectra and EEM fluorescence spectra

The absorption and EEM spectra of the WSOC and MSOC samples were analyzed using a UV-Vis spectrophotometer (UV-4802; Unico, China) and an Aqualog fluorometer (Horiba Scientific, USA), respectively. The wavelengths used to characterize the UV-Vis spectra were between 200 to 800 nm at a step size of 2 nm. Purified water was used as a baseline correction before measure. Mass absorption efficiency (MAE, m^2 g^{-1} C) can be obtained as following equation (Li et al., 2018):

$$MAE_\lambda = A_\lambda \bullet \ln(10) / (C \bullet L) \quad (1)$$

https://doi.org/10.5194/acp-2019-584
Preprint. Discussion started: 7 August 2019

Atmospheric Chemistry and Physics Discussions

Here, A_λ is the value of light absorption at given wavelength given by the spectrophotometer; C (μg C mL^{-1}) is the concentration of WSOC and MSOC fractions; L is the optical path length. Moreover, the pH of WSOC fraction was measured for all samples within the range of 5.5-6.5, generally thought it didn't affect the absorbance according to prior study (Chen et al., 2016a).

The emission and excitation wavelengths of the fluorescence spectra were from 245 to 580 nm and 240 to 500 nm, respectively. The wavelength increments of the emission and excitation scans were 4.66 and 3 nm, respectively. Further, we subtracted the contributions of the solvents to the fluorescence spectra.

2.4 Ultrahigh resolution ESI FT-ICR MS analysis

Two fractions of six samples (IDs: 18 and 23 represented the mean fluorescence level of biomass burning; IDs: 38 and 46 represented anthracite and bituminous coal, respectively; IDs: 55 represents a day's worth of samples of tunnel inlet and outlet, and IDs: 59 represents direct vehicle exhaust) were selected for FT-ICR MS analysis. To remove inorganic ions prior to instrumental analysis, the WSOC fraction was further adjusted to pH = 2 by the addition of hydrochloric acid (HCl), and then passed through a solid-phase extraction cartridge (Oasis HLB, 30 um, 60 mg/cartridge; Waters Corporation, USA). The constituent retained on the SPE cartridge were eluted with methanol containing 2% ammonia (v/v). Eluted samples were evaporated until dry under a gentle nitrogen gas stream. The extract by methanol was also evaporated under a gentle nitrogen gas stream for preparation.

We used the analysis method of FT-ICR MS described in detail in one of our previous studies (Mo et al., 2018). Briefly, ultrahigh resolution mass spectra were obtained using a solariX XR FT-ICR MS (Bruker Daltonics GmbH, Bremen, Germany) equipped with a 9.4-T superconducting magnet and an ESI ion source. The system was operated in negative ionization mode. The ion accumulation time was set to 0.6 s. The lower and upper mass limit was set to m/z 150 and 800 Da, respectively. The mass spectra were externally calibrated with arginine clusters using a linear calibration and then internally recalibrated with typical O_6S_1 class species peaks using

https://doi.org/10.5194/acp-2019-584
Preprint. Discussion started: 7 August 2019


Atmospheric Chemistry and Physics Discussions

quadratic calibration in DataAnalysis ver. 4.4 software (Bruker Daltonics). A typical mass-resolving power >450 000 at m/z 319 with <0.2 ppm absolute mass error was achieved. The mass spectra of field blank filters were analyzed to detect possible contamination following the same procedures. More data processing was presented in S1 of supplement.

2.5 PARAFAC analysis for EEM spectra

Parallel factor (PARAFAC) analysis with non-negativity constrains was used to explore the fluorescent components in dissolved BrC based on the method established by Murphy et al (Murphy et al., 2013;Andersson and Bro, 2000), which was performed using drEEM toolbox version 2.0 using a MATLAB software (http://models.life.ku.dk/drEEM). This method had been widely applied to the analysis of fluorescence spectra in aerosol (Chen et al., 2016b;Chen et al., 2016a;Matos et al., 2015;Wu et al., 2019). Absorbance measurements was used to correct the EEMs for inner filter effects (IFE) according to the previous studies (Luciani et al., 2009;Gu and Kenny, 2009;Fu et al., 2015). The highest light absorbance in the calibrated wavelength range in two fractions was not greater than 2 (mostly below 1 at 254 nm), which is appropriate for the inner filter corrections of the EEMs (Gu and Kenny, 2009;Murphy et al., 2013). Each EEM was normalized to the Raman peak area of purified water collected on the same day to correct fluorescence in Raman Units (RU) at excitation 350 nm, and corrected for the dilution factor (Murphy et al., 2013;Murphy et al., 2010). Additional, the signals of the first-order and second-order Rayleigh and Raman scattering in the EEM were removed by using an interpolation method (Bahram et al., 2006). Repeated convergence of the model was examined based on the iteration of the minimum squares principle. The exploration phases of 2- to 7-componet PARAFAC models were contained that evaluation of the shape of spectral loading, leverage analysis, examination of the core consistency, residual analysis, and split half analysis (Figure S2-S7). Finally, six component PARAFAC model was identified and successfully passed the split analysis

https://doi.org/10.5194/acp-2019-584
Preprint. Discussion started: 7 August 2019

Atmospheric Chemistry and Physics Discussions

with the split style of "$S_4C_6T_3$" for WSOC and MSOC fraction in 60 samples, respectively.

3 Results and discussion

3.1 Emission Characteristics and Optical Properties of Extracts.

The PM, OC, and EC emission factors (EFs) of 27 biomass and 17 coal combustion experiments are summarized in Table S3. The relevant EFs of some of the biomass species were reported previously (Cui et al., 2018). In the current experiment, the EFs of PM, OC, and EC from burning 27 types of biomass were 15 ± 11 g kg^{-1} fuel, 8.0 ± 6.4 g kg^{-1} fuel, and 7.7 × 10^{-1} ± 3.4 × 10^{-1} g kg^{-1} fuel, respectively. The EFs emitted from bituminous coal combustion (PM = 9.1 × 10^{-1} ± 6.5 × 10^{-1} g kg^{-1} fuel, OC = 4.2 × 10^{-1} ± 3.3 × 10^{-1} g kg^{-1} fuel, EC = 9.4 × 10^{-2} ± 1.9 × 10^{-1} g kg^{-1} fuel) were much higher than those of anthracite combustion (PM = 1.5 × 10^{-1} ± 8.9 × 10^{-2} g kg^{-1} fuel, OC = 1.2 × 10^{-2} ± 4.5 × 10^{-3} g kg^{-1} fuel, EC = 1.6 × 10^{-4} ± 1.4 × 10^{-4} g kg^{-1} fuel) in the same stove. These differences can be attributed to the high volatile matter content of bituminous coal (Tian et al., 2017;Chen et al., 2005). Note that coal smoke was collected when the fire had been ignited using one third of the material, after which the remaining part was added. Thus, the results of our study were lower than the real values.

Mass absorption efficiency (MAE) can be used to characterize the efficiency of solar energy absorption, which is represented by the degree of conjugation and the amount of electron delocalization in molecules (Chen et al., 2016a). As shown in Figures 2b and S8b, and in Table S4, MAE at 365 nm (MAE_{365}) is significantly higher in the case of biomass burning and coal combustion than in vehicle emissions in the current study. Higher MAE_{365} values were observed in the MSOC fractions collected from biomass burning (2.3 ± 1.1 m^2 $g^{-1}C$) and bituminous coal combustion (3.2 ± 1.1 m^2 $g^{-1}C$) compared to their WSOC fraction values. This may be due to the fact that these strongly light-absorbing fat-soluble components are likely to be large molecular weight PAHs, and quinones from biomass burning and fossil fuel combustion (Sun et al., 2007;Chen and Bond, 2009), while we obtained the opposite results in the case of

https://doi.org/10.5194/acp-2019-584
Preprint. Discussion started: 7 August 2019

Atmospheric Chemistry and Physics Discussions

anthracite combustion and vehicle emissions. Moreover, the higher MAE_{365} in biomass burning and bituminous coal combustion represented a stronger absorbing ability in the case of the MSOC fraction, which reflected greater variation in the chemical composition than in the WSOC fraction. The MAE_{365} of biomass burning and coal combustion in the WSOC fraction was also higher than that of ambient aerosol and biomass and coal combustion experiments in a laboratory sampling system (Chen et al., 2018;Zhu et al., 2018;Yan et al., 2015;Li et al., 2018;Park and Yu, 2016) (Figure S4).

3.2 EEM spectra of dissolved BrC.

We applied the PARAFAC model (Murphy et al., 2013) to determine the underlying chromophore components of the 60 emission source samples. Six typically independent components of the WSOC fraction were resolved, as shown in the top of Figure 1 and Table 1. Compared with the previous studies, the EEM of P1 and P6 were similar to those for 7CM-C1 (the C1 component of a seven-component model) and 7CM-C3, pertaining to water-extracted matter in urban and forest area, and marine aerosols, in Japan (Chen et al., 2016b). Further, there were peaks in the emission wavelengths (> 400 nm) of P1 and P6, which were probably derived from conjugated systems (Chen et al., 2016b). The peak of the P3 component was almost located in region IV, which was categorized as a protein-like (cytidine) or tryptophan-like (peak T) fluorophore (Qin et al., 2018;Fan et al., 2016). Generally, peaks at shorter excitation wavelengths (< 250 nm) and shorter emission wavelengths (< 350 nm) are correlated with simple aromatic proteins such as tyrosine (Cory and Mcknight, 2005), which is quite similar to the peak of the P2 component observed in this study. According to a prior report, the spectra of the P5 component was also similar to tryptophan- and tyrosine-like components (Chen et al., 2017a). The spectra of the P4 component has been reported relatively rarely but is similar to previously observed peaks that are considered to arise mainly in surface water and algal secretions (Yu et al., 2015). Note that the origins and chemical structures of the

https://doi.org/10.5194/acp-2019-584
Preprint. Discussion started: 7 August 2019

Atmospheric Chemistry and Physics Discussions

chromophores studied are not necessarily similar to those of chromophores with the same names in other types of organic matter.

Table 1. The maximum excitation and emission wavelengths of the PARAFAC components from the WSOC and MSOC fractions extracted from three origins

	PARAFAC component	Excitation maxima (nm)	Emission maxima (nm)	Assignment according to published papers	References
WSOC	P1	251, 314	415	HULIS-1, terrestrial humic-like component	(Chen et al., 2016b;Sgroi et al., 2017;Fu et al., 2015)
	P2	254	337	Tyrosine-like	(Cory and Mcknight, 2005)
	P3	287	360	Protein-like (cytidine) or tryptophan-like	(Qin et al., 2018;Fan et al., 2016)
	P4	251	374	-	-
	P5	278	319	Protein-like fluorophores	(Fu et al., 2015)
	P6	254, 371	485	HULIS-1, conjugated systems, a terrestrial humic or fulvic acid-like component	(Chen et al., 2016b)
MSOC	C1	308	356	-	
	C2	<250,272	388		
	C3	<250	434	C2 for the urban ASOM samples	(Matos et al., 2015)
	C4	257	360		
	C5	284	328		
	C6	269	310		

https://doi.org/10.5194/acp-2019-584
Preprint. Discussion started: 7 August 2019

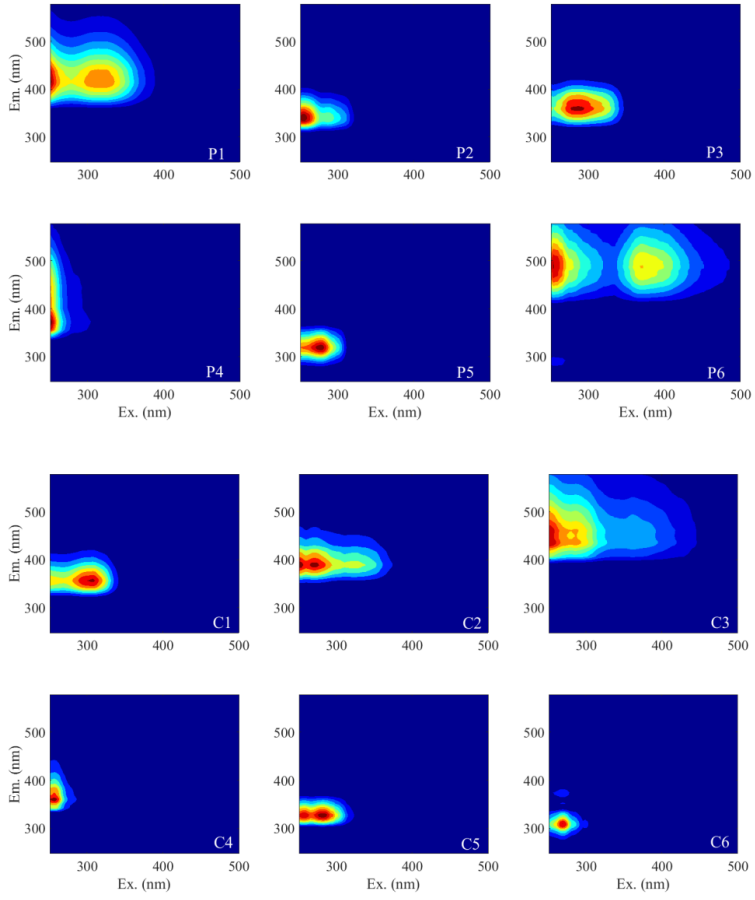

Figure 1. The excitation-emission matrix (EEM) components spectra determined by parallel factor (PARAFAC) analysis of WSOC (top: P1-P6) and MSOC (bottom: C1-C6) extracted from three origins.

The results from the six-component model (abbreviated C1–6) of the MSOC fractions identified by PARAFAC, as described in the bottom of Table 1 and Figure 1, were obviously different to those obtained for the WSOC fraction. The peak of C1 component was similar to that of the P3 component of the WSOC fraction, but the excitation wavelength was higher, which indicated the presence of conjugated unsaturated bond systems shifting towards the high wavelengths of the C1 component (Matos et al., 2015). Moreover, as reported in a previous study, the C3 component was similar to the C2 component of urban alkaline-soluble organic matter (ASOM)

https://doi.org/10.5194/acp-2019-584
Preprint. Discussion started: 7 August 2019


Atmospheric Chemistry and Physics Discussions

samples collected from the city of Aveiro, Portugal (Matos et al., 2015). Because the fluorescence spectrum of the MSOC fraction was poorly characterized, the molecular composition of the other fluorescent components was studied using FT-ICR MS.

The maximum fluorescence intensities (F_{max}) (Table S5, S6) is calculated by multiplying the maximum excitation loading and maximum emission loading for each component by its score (Murphy et al., 2013). Generally, changes in the relative abundance of a component ($F_{max}/\sum F_{max}$) could indicate changes in its overall importance, which had been successful applied to study the origins of chromophores (Yan and Kim, 2017;Chen et al., 2017a;Chen et al., 2016b;Wu et al., 2019). In the current study, the relative intensities of different fluorescent components in different types of samples was highly variable, depending on the sources. As shown in Figure 2a, P1 component was intense in the case of vehicle emission, accounting for an average of 30 ± 8.3% of the total fluorescence intensities of vehicle emission. P2 and P4 components were intense in the cases of biomass burning (mean: 33 ± 11% of fluorescence intensities of biomass burning) and coal combustion (mean: 34 ± 7.7%), respectively. The P3 components were almost equal across all samples. The possible reason is that the P3 components is similar to tryptophan-like compounds, where these are common to practically all published models and are likely to be found in almost all sources (Yu et al., 2015). It was obvious that P5 component was intense in direct vehicle exhaust (IDs: 59 and 60; mean: 30 ± 1.6%). In contrast, the fluorescence of P6 components was weak in any of the samples, but the P6 component in vehicle emissions (mean: 9.4 ± 2.2%) significantly exceeded those of biomass burning and coal combustion (both 2.5%). The above results clearly indicates that the chemical composition of chromophoric water-soluble BrC varies remarkably among sources.

https://doi.org/10.5194/acp-2019-584
Preprint. Discussion started: 7 August 2019

Atmospheric Chemistry and Physics Discussions

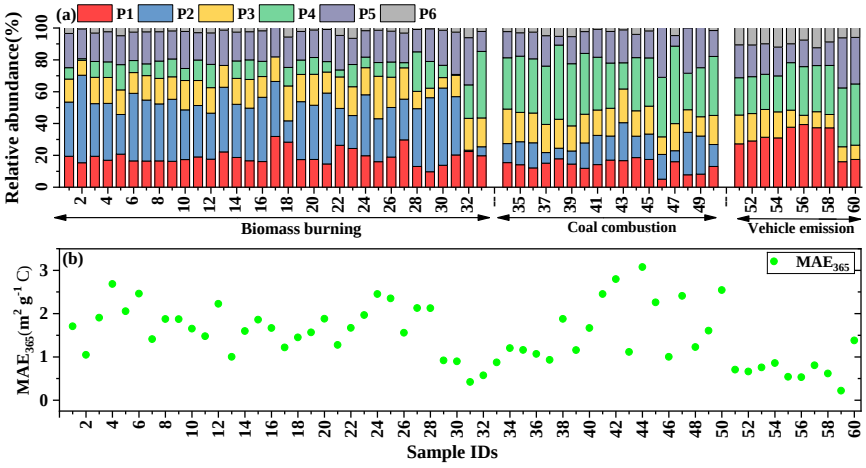

Figure 2. (a) Relative abundance of each PARAFAC component, (b) mass absorption efficiency at 365 nm (MAE_{365}) values in WSOC fractions from three origins

The relative intensities of the fluorescent components in the MSOC fraction exhibit similar characteristics to the WSOC fraction (Figure S8a). The C1 and C2 components was the substances with more intense in the case of biomass burning (mean: 38 ± 14 % and 21 ± 6.9%, respectively). C4 components was intense in samples of coal combustion (mean: 41 ± 6.0%). The levels of component C3 were not abundance between the three types of fuel tested. The C5 and C6 components was more intense in direct vehicular exhaust (IDs: 59 and 60; mean: 25 ± 6.8% and 50 ± 6.8%, respectively). Combining these results with the above-mentioned WSOC results and comparing the different characteristics and fuel source information, the fluorescent components obtained by EEM-PARAFAC can potentially assist with source apportionment for environmental monitoring applications.

3.3 Molecular composition of FT-ICR MS and chemical structures of chromophores

The relative abundances of the four compound groups (CHO, CHON, CHOS, and CHONS) in the WSOC fraction are presented in Figure S9. These results were consistent with previous results (Song et al., 2018), in which S- containing compounds were mainly found in coal combustion emissions. Conversely, our results

https://doi.org/10.5194/acp-2019-584
Preprint. Discussion started: 7 August 2019


Atmospheric Chemistry and Physics Discussions

proved that N-containing substances were also abundant in coal combustion aerosols. One possible reason for this concerns the viable coal types; for example, significant differences were observed between water-extracts of IDs 36 (anthracite coal) and 46 (bituminous coal). More detailed information about the molecular compositions is provided in Tables S7 and S8, and Figure S10, S11 and S12.

The previous study reported that potential BrC chromophores were identified by determining those compounds in the region between Double bond equivalent (DBE) = 0.5 × C and DBE = 0.9 × C (in the coordinate axis, the x-axis is the C number and the y-axis is the DBE value) (Lin et al., 2018). To explore the possible chemical structures of dissolved chromophores, the methods of the O/C and H/C ratios of matter or functional groups were used to classify the ion groups of FT-ICR MS as listed in Figure 2. Furthermore, according to the all ions or potential BrC ions, there are total four classifications. The first method is to follow their O/C and H/C ratios of matter to classify all ions of FT-ICR MS; the second method is to follow their O/C and H/C ratios of matter to classify potential BrC ions; the third method is to follow their functional groups to classify all ions; the last method is to follow their functional groups to classify potential BrC ions. The relationship between the relative intensities of classified group of ions (the ratio of intensities of each ion group to total ion intensities) and the relative abundance of fluorescent components were presented in Table S9-S16. The results indicated that the method that sorted the potential BrC ion groups by their functional groups is best for explaining the relationship between the chemical composition and fluorescent components. For example, the presence of L-CHON groups with O/N $\leq$ 2 suggests that these reduced N compounds may be associated with alkyl amides and alkyl nitrile, as well as heterocyclic aromatic compounds with single N atoms (Alexander et al., 2009;Song et al., 2018). The H-CHON group with O $\geq$ 3, O/N > 2 and AI_{mod} > 0.5 suggests that these compounds contain O and N atoms, such as benzene rings substituted with O-containing groups (hydroxyl, and carboxyl) and nitro-aromatics (Chen et al., 2016b;Song et al., 2018;Lin et al., 2016). The H-CHOS group had O/S $\geq$ 4, suggesting the assignment of a sulfate group (-OSO_3H). As sulfate groups carry four oxygen atoms and readily deprotonate

https://doi.org/10.5194/acp-2019-584
Preprint. Discussion started: 7 August 2019

Atmospheric Chemistry and Physics Discussions

394 in ESI, they are more likely to be organosulfates (Jiang et al., 2016). The presence of
395 the H-CHONS group suggested not only the assignment of a sulfate group (-OSO_3H),
396 but also an additional one or two nitrooxy groups (-ONO_2) (Mo et al., 2018).

397 **Table 2**. The classification methods of ion groups of FT-ICR MS

Specific classification methods			
Function groups		H/C and O/C[a]	
CHO_1	O_1	Lipids	O/C=0-0.2, H/C=1.7-2.2
$CHO_{>1}$	$O_{>1}$	Proteins	O/C=0.2-0.6, H/C=1.5-2.2, N/C ≥ 0.05
L-CHON	O/N ≤ 2	H-Lignin	O/C = 0.1−0.6, H/C =0.6−1.7, 0.5 < AI_{mod} < 0.67
H-CHON	O/N > 2	M-Lignin	O/C = 0.1−0.6, H/C =0.6−1.7, 0 < AI_{mod} ≤ 0.5, DBE ≥ 4
L-CHOS	O/S < 4	L-Lignin	O/C = 0.1−0.6, H/C =0.6−1.7, 0 < AI_{mod} ≤ 0.5, DBE < 4
H-CHOS	O/S ≥ 4	Carbohydrates	O/C = 0.6−1.2, H/C = 1.5−2.2
L-CHONS	O/S < 7(N_1); O/S < 10 (N_2)	Tannins	O/C = 0.6−1.2, H/C = 0.5−1.5, AI_{mod} < 0.67
H-CHONS	O/S ≥ 7(N_1); O/S ≥ 10 (N_2)	Unsaturated hydrocarbons	O/C = 0−0.1, H/C = 0.7−1.5

398 Note that L, M, and H stands for low, moderate, and high, respectively; The lignin group is further divided into three subcategories on the base of their AI_{mod} and
399 DBE (H-Lignin: 0.5 < AI_{mod} < 0.67; M-Lignin: 0 < AI_{mod} ≤ 0.5, DBE ≥ 4; L-Lignin: 0 < AI_{mod} ≤ 0.5, DBE < 4).
400 a: (Patriarca et al., 2018)

https://doi.org/10.5194/acp-2019-584
Preprint. Discussion started: 7 August 2019

Atmospheric Chemistry and Physics Discussions

401

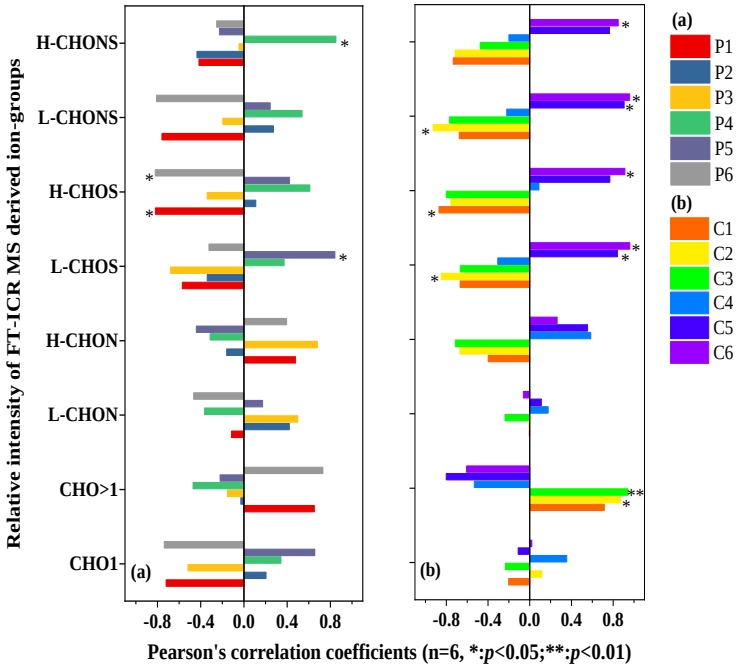

402

403

404 **Figure 3.** Pearson's correlation coefficients (r) and significance levels (two-sided t-test) obtained
405 from the correlation analysis between the relative intensity of the ion groups based on
406 Fourier-transform ion cyclotron resonance mass spectrometry (FT-ICR MS), and the relative
407 intensity of the (a) six components of the WSOC fractions and (b) six components of the MSOC
408 fractions.

409 **3.3.1 Composition of chromophores of WSOC**

410 The relationship between the relative intensities of the classified ion groups of FT-ICR
411 MS and the relative contents of the PARAFAC components in the WSOC fraction
412 were presented in Figure 3a and Table S15. The P1 and P6 components were both
413 negatively correlated with the H-CHOS group ($p < 0.05$). Considering that P1 and P6
414 components was intense in samples of vehicle emissions, the main compounds
415 detected from this source were O_4S_1–$O_{12}S_1$ class species with a wide range of C
416 numbers (7–34) and double bonds equivalent (DBE) values (4–20), of which O_4S_1 and

https://doi.org/10.5194/acp-2019-584
Preprint. Discussion started: 7 August 2019

Atmospheric Chemistry and Physics Discussions

O_5S_1 class species, which exhibit an R-OSO_3H structure, were the most abundant. Among these chemical formulas, we found that many aromatic organosulfate isomers with relatively high DBE values (≥ 4) were side chains or aromatic rings, and thus their chemical formulas could be those of alkylbenzene rings substituted with one sulfate and one hydroxyl group (Song et al., 2018), such as $C_8H_{10}O_5S$ (DBE: 4) and $C_{10}H_{10}O_6S$ (6). These structures were detected in humic-like substances (HULIS) from coal-smoke and SOA generated under all experimental conditions (Riva et al., 2015;Song et al., 2018) and were likely responsible for the P1 and P6 components.

The P4 component was positively correlated with the H-CHONS group (p < 0.05), suggesting nitrooxy-organosulfates (nitrooxy-OS) (Mo et al., 2018). Nitrooxy-OS is probably be formed by photooxidation of biogenic VOCs in smog chamber experiments conducted under high nitrogen oxide (NO_x) concentrations (Lin et al., 2012). These results indicate that coal combustion is an important source of nitrooxy-OS, and this conclusion was consistent with the results of previous studies (Song et al., 2018). As shown in Figure 4, a wide range of C number (6–32) and DBE values (3–23) were observed in this group, and the DBE value increased with the C number. The main compounds in this group were $O_7N_1S_1$–$O_{13}N_1S_1$ class species, with $O_7N_1S_1$ class species being the most abundant. It is worth noting that most of the H-CHONS compounds had DBE values greater than or equal to 4, and the compounds with high intensities in the H-CHONS groups detected from coal combustion were $C_6H_5O_7NS$ (5), $C_{10}H_7O_7NS$ (8), and $C_{10}H_6O_{11}N_2S$ (9). The most likely structure of these compounds is a benzene ring substituted with one sulfate and one or two nitrooxy groups (Song et al., 2018;Jiang et al., 2016). These were also detected in high concentrations in aerosols from Belgium and on a heavy $PM_{2.5}$ haze day in Beijing city (Jiang et al., 2016;Kahnt et al., 2013).

The presence of the P5 component was highly correlated with the L-CHOS group (p < 0.05). This group was mainly composed of O_3S and O_7S_2 class species from direct vehicle exhaust emissions. Generally, these compounds contained too little oxygen to form sulfate functional groups, containing reduced sulfur (S), such as sulfonates, which was also detected in cloud water (Zhao et al., 2013). In these groups,

https://doi.org/10.5194/acp-2019-584
Preprint. Discussion started: 7 August 2019

Atmospheric Chemistry and Physics Discussions

the main compounds of $C_{26}H_{24}O_3S$ (15), $C_{27}H_{26}O_3S$ (15), and $C_{25}H_{22}O_3S$ (15) were homologues of $C_{24}H_{20}O_3S$ (15), with the same general formula, $C_nH_{2n-28}SO_3$, and DBE values, of 15, likely corresponding to sulfonates of substituted benzopyrene ($C_{20}H_{12}$, DBE=15) (Blair et al., 2017). However, the P2 and P3 components were not significantly correlated with these ion groups.

3.3.2 Composition of chromophores of MSOC

Figure 3b and Table S16 show the relationship between the relative intensity of the classified ions groups and the relative contents of the PARAFAC components of the MSOC fraction. Only the C1 and C3 components were associated with one ion group (H-CHOS and $CHO_{>1}$, respectively). Considering that the C1 component was highly intense in the case of biomass burning, the H-CHOS groups observed in samples of biomass burning were O_5S_1, O_7S_1, $O_{10}S_2$, $O_{13}S_1$ class species, of which $O_{10}S_2$ was the most abundant family. The probable structure of these species is an organosulfate with other O-containing functional groups, such as hydroxyl or carboxyl groups. This groups had a narrow range of C numbers (12–16) and DBE values (8), such as $C_{14}H_{14}O_{10}S_2$ (8) and its homologues $C_{13}H_{12}O_{10}S_2$ (8), $C_{15}H_{16}O_{10}S_2$ (8), as well as $C_{15}H_{16}O_7S$ (8), $C_{16}H_{18}O_7S$ (8), $C_{12}H_{10}O_{13}S$ (8), and $C_{13}H_{12}O_{13}S$ (8).

C2 component was positively correlated with $CHO_{>1}$, and negatively correlated with L-CHOS and L-CHONS groups. Figure 5 presented the DBE versus C number for the $CHO_{>1}$ group from samples of biomass burning, with the main compounds had C numbers of 17–20, DBE (10–11), and O numbers of 4–5. The potential structures of $C_{18}H_{16}O_4$ (11) and $C_{17}H_{16}O_4$ (10) are indicated as a and b, respectively, in Figure 5 and are suspected to be cyclic esters. The L-CHOS group were mainly O_4S_2 class species, of which $C_{12}H_{10}O_4S_2$ (8) was the main formula. The possible chemical structure is of two S-heterocycles connected to two ester bonds. Thus, C2 components may relate to ester compounds.

Further, the C5 component was positively correlated with L-CHOS and L-CHONS groups ($p < 0.05$), and the C6 component was positively associated with all S-containing groups ($p < 0.05$). We list some of the main formulas of these groups

https://doi.org/10.5194/acp-2019-584
Preprint. Discussion started: 7 August 2019

Atmospheric Chemistry and Physics Discussions

detected in direct vehicle exhaust (IDs: 59), such as $C_{12}H_{12}O_7S_2$ (7) and $C_{13}H_{14}O_7S_2$ (7) for L-CHOS groups; $C_{14}H_{14}O_{10}S_2$ (8) and $C_{15}H_{16}O_{10}S_2$ (8) for H-CHOS; $C_{36}H_{23}O_4NS$ (26) for L-CHONS; and $C_{10}H_6O_{11}N_2S$ (9), $C_{11}H_8O_{11}N_2S$ (9), $C_{10}H_7O_{13}NS$ (8), $C_{11}H_9O_{13}NS$ (8), $C_{12}H_{11}O_{13}NS$ (8) and $C_{12}H_8O_{14}N_2S$ (10) for H-CHONS. The L-CHOS groups containing two S atoms is potential to be formed by sulfonation reactions, and their possible structure is of a fused benzene ring substituted with two sulfonates ($-SO_3H$). $C_{36}H_{23}O_4NS$ may contain substantial quantities of S-containing compounds with reduced N (e.g., amide and nitrile, and heterocyclic aromatics) (Song et al., 2018). These results indicate that the C5 component is potentially related to sulfonates, but the structure of the C6 component is unclear. However, C4 components did not correlate with ion groups. Note that one class of compounds contributed to several fluorescent components, which indicated that numerous functional groups affect each component individually.

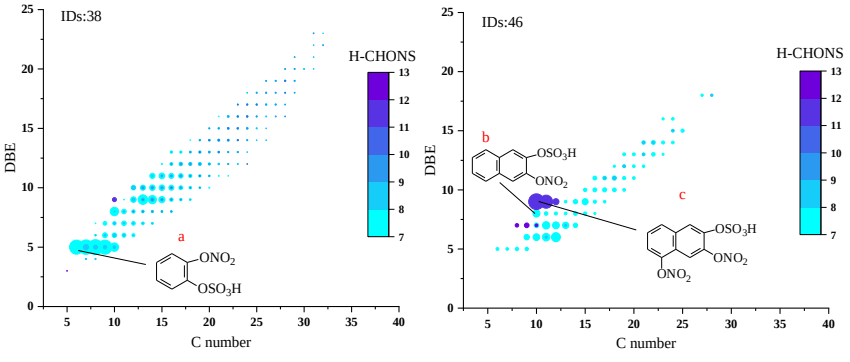

Figure 4. Double bond equivalent (DBE) versus C number for the H-CHONS group of WSOC of coal combustion samples. The color bar and marker size denote the number of O atoms and the relative intensities of the compounds; a: $C_6H_5O_7NS$ (DBE: 5); b: $C_{10}H_7O_7NS$ (8); and c: $C_{10}H_6O_{11}N_2S$ (9).

https://doi.org/10.5194/acp-2019-584
Preprint. Discussion started: 7 August 2019

Atmospheric Chemistry and Physics Discussions

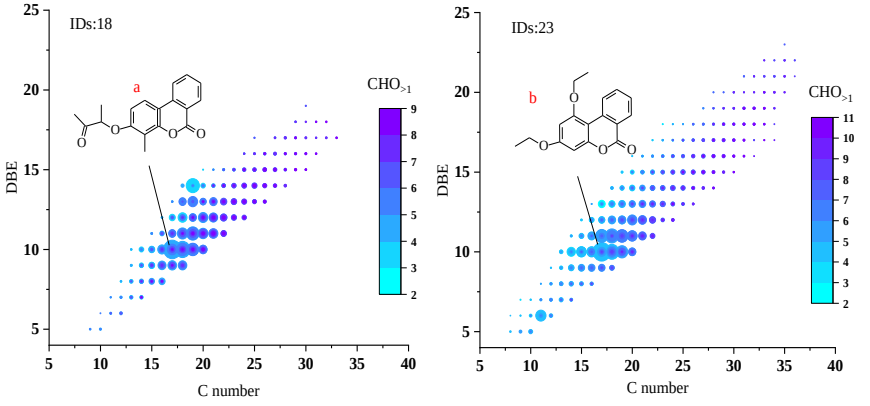

Figure 5. The DBE versus C number for the $CHO_{>1}$ group of MSOC of biomass burning samples. The color bar and marker size denote the number of O atoms and the relative intensities of the compounds, a: $C_{18}H_{16}O_4$ (11); b: $C_{17}H_{16}O_4$ (10).

4 Conclusions

We conducted comprehensive measurements on light absorption, fluorescence, and molecular compositions of dissolved BrC derived from smoke particles during the simulated combustion of biomass and coal, as well as vehicle emissions. We observed the optical properties of the WSOC and MSOC fractions and observed that the light absorption of methanol-soluble BrC was stronger. Six fluorescent components were resolved in the WSOC and MSOC fractions by PARAFAC analysis, respectively. The relative intensities of the fluorescent components of the WSOC and MSOC fractions mainly depended on the different types of smoke particles, which were derived from several origins, suggesting that the fluorescent components varied from source to source. This result may be useful for fluorescence-based methods, which play an important role in the classification and source identification of BrC dissolved in the atmosphere.

We also discussed the possible structures of these chromophores. Our results indicate that these fluorescent components were mainly affected by functional groups, especially functional groups containing N and S. In the case of the WSOC fraction, P1 and P6 components were mainly associated with aromatic organosulfate compounds;

https://doi.org/10.5194/acp-2019-584
Preprint. Discussion started: 7 August 2019

Atmospheric Chemistry and Physics Discussions

the P4 and P5 components were mainly associated with nitrooxy-OS compounds and sulfonates, respectively. However, we did not elucidate the structures of the P2 and P3 components. In the case of the MSOC fraction, the C1 component was mainly related to organsulfate compounds; the C3 component was related to $CHO_{>1}$ groups; the C2 component was mainly correlated with esters; and the C5 component was related to sulfonates. The C6 component was correlated well with S-containing compounds. As with the P2 and P3 components, we know little about the structure of the C4 component. Our findings provide insights into the chemical structures of water- and methanol-soluble chromophores, and these results may be useful for further aerosol studies, for source apportionment of dissolved BrC based on EEM fluorescence.

Data availability. The data used in this study are available upon request; please contact Gan Zhang (Zhanggan@gig.ac.cn) and Jun Li (junli@gig.ac.cn)

Supplement. The supplement related to this article is available.

Author contributions. JT, GZ, JL, and YC designed the experiment. JT and MC carried out the measurements and analyzed the data. JT, TS, YH, and HJ organized and performed the samplings. JT (Jianhui Tang) and BJ supported the fluorescence and FT-ICR MS instrument. JT wrote the paper. JL, YM, JS, PP, and GZ reviewed and commented on the paper.

Competing interests. The authors declare that they have no conflict of interest.

Acknowledgements. This study was supported by the Natural Science Foundation of China (NSFC; Nos. 41430645 and 41773120), the National Key R&D Program of China (2017YFC0212000), and the International Partnership Program of Chinese Academy of Sciences (Grant No.132744KYSB20170002).

Reference:

Alexander, L., Smith, J. S., and Julia, L.: Molecular characterization of nitrogen-containing

https://doi.org/10.5194/acp-2019-584
Preprint. Discussion started: 7 August 2019

Atmospheric Chemistry and Physics Discussions

organic compounds in biomass burning aerosols using high-resolution mass spectrometry, Environ. Sci. Technol., 43, 3764-3771, https://doi.org/10.1021/es803456n, 2009.

Andersson, C. A., and Bro, R.: The N-way Toolbox for MATLAB, Chemom. Intell. Lab. Syst., 52, 1-4, https://doi.org/10.1016/s0169-7439(00)00071-x, 2000.

Andrade-Eiroa, Á., Canle, M., and Cerdá, V.: Environmental Applications of Excitation-Emission Spectrofluorimetry: An In-Depth Review I, Appl. Spectrosc. Rev., 48, 1-49, https://doi.org/10.1080/05704928.2012.692104, 2013.

Bahram, M., Bro, R., Stedmon, C., and Afkhami, A.: Handling of Rayleigh and Raman scatter for PARAFAC modeling of fluorescence data using interpolation, J. Chemom., 20, 99-105, https://doi.org/10.1002/cem.978, 2006.

Bhattacharya, R., and Osburn, C. L.: Multivariate Analyses of Phytoplankton Pigment Fluorescence from a Freshwater River Network, Environ. Sci. Technol., 51, 6683-6690, https://doi.org/10.1021/acs.est.6b05880, 2017.

Blair, S. L., MacMillan, A. C., Drozd, G. T., Goldstein, A. H., Chu, R. K., Pasa-Tolic, L., Shaw, J. B., Tolic, N., Lin, P., Laskin, J., Laskin, A., and Nizkorodov, S. A.: Molecular Characterization of Organosulfur Compounds in Biodiesel and Diesel Fuel Secondary Organic Aerosol, Environ. Sci. Technol., 51, 119-127, https://doi.org/10.1021/acs.est.6b03304, 2017.

Chen, H., Liao, Z. L., Gu, X. Y., Xie, J. Q., Li, H. Z., and Zhang, J.: Anthropogenic Influences of Paved Runoff and Sanitary Sewage on the Dissolved Organic Matter Quality of Wet Weather Overflows: An Excitation-Emission Matrix Parallel Factor Analysis Assessment, Environ. Sci. Technol., 51, 1157-1167, https://doi.org/10.1021/acs.est.6b03727, 2017a.

Chen, Q., Ikemori, F., and Mochida, M.: Light Absorption and Excitation-Emission Fluorescence of Urban Organic Aerosol Components and Their Relationship to Chemical Structure, Environ. Sci. Technol., 50, 10859-10868, https://doi.org/10.1021/acs.est.6b02541, 2016a.

Chen, Q., Miyazaki, Y., Kawamura, K., Matsumoto, K., Coburn, S., Volkamer, R., Iwamoto, Y., Kagami, S., Deng, Y., Ogawa, S., Ramasamy, S., Kato, S., Ida, A., Kajii, Y., and Mochida, M.: Characterization of Chromophoric Water-Soluble Organic Matter in Urban, Forest, and Marine Aerosols by HR-ToF-AMS Analysis and Excitation-Emission Matrix Spectroscopy, Environ. Sci. Technol., 50, 10351-10360, https://doi.org/10.1021/acs.est.6b01643, 2016b.

Chen, Q., Ikemori, F., Nakamura, Y., Vodicka, P., Kawamura, K., and Mochida, M.: Structural

https://doi.org/10.5194/acp-2019-584
Preprint. Discussion started: 7 August 2019

Atmospheric Chemistry and Physics Discussions

and Light-Absorption Characteristics of Complex Water-Insoluble Organic Mixtures in Urban Submicrometer Aerosols, Environ. Sci. Technol., 51, 8293-8303, https://doi.org/10.1021/acs.est.7b01630., 2017b.

Chen, Y., Sheng, G., Bi, X., Feng, Y., Bixian Mai, A., and Fu, J.: Emission Factors for Carbonaceous Particles and Polycyclic Aromatic Hydrocarbons from Residential Coal Combustion in China, Environ. Sci. Technol., 39, 1861-1867, https://doi.org/10.1021/es0493650, 2005.

Chen, Y., and Bond, T. C.: Light absorption by organic carbon from wood combustion, Atmos. Chem. Phys., 10, 1773-1787, https://doi.org/10.5194/acp-10-1773-2010, 2009.

Chen, Y., Ge, X., Chen, H., Xie, X., Chen, Y., Wang, J., Ye, Z., Bao, M., Zhang, Y., and Chen, M.: Seasonal light absorption properties of water-soluble brown carbon in atmospheric fine particles in Nanjing, China, Atmos. Environ., 230-240, https://doi.org/10.1016/j.atmosenv.2018.06.002, 2018.

Coble, P. G.: Characterization of marine and terrestrial DOM in seawater using excitation-emission matrix spectroscopy, Mar. Chem., 51, 325-346, https://doi.org/10.1016/0304-4203(95)00062-3, 1996.

Cory, R. M., and Mcknight, D. M.: Fluorescence Spectroscopy Reveals Ubiquitous Presence of Oxidized and Reduced Quinones in Dissolved Organic Matter, Environ. Sci Technol., 39, 8142-8149, https://doi.org/10.1021/es0506962, 2005.

Cui, M., Chen, Y., Zheng, M., Li, J., Tang, J., Han, Y., Song, D., Yan, C., Zhang, F., Tian, C., and Zhang, G.: Emissions and characteristics of particulate matter from rainforest burning in the Southeast Asia, Atmos. Environ., 191, 194-204, https://doi.org/10.1016/j.atmosenv.2018.07.062, 2018.

Dai, S., Bi, X., Chan, L. Y., He, J., Wang, B., Wang, X., Peng, P., Sheng, G., and Fu, J.: Chemical and stable carbon isotopic composition of PM2.5 from on-road vehicle emissions in the PRD region and implications for vehicle emission control policy, Atmos. Chem. Phys., 15, 3097-3108, https://doi.org/10.5194/acp-15-3097-2015, 2015.

Fan, X., Song, J., and Peng, P. a.: Comparison of isolation and quantification methods to measure humic-like substances (HULIS) in atmospheric particles, Atmos. Environ., 60, 366-374, https://doi.org/10.1016/j.atmosenv.2012.06.063, 2012.

https://doi.org/10.5194/acp-2019-584
Preprint. Discussion started: 7 August 2019

Atmospheric Chemistry and Physics Discussions

600 Fan, X., Wei, S., Zhu, M., Song, J., Peng, P: Comprehensive characterization of humic-like
601 substances in smoke PM2.5 emitted from the combustion of biomass materials and fossil fuels,
602 Atmos. Chem. Phys., 16, 13321-13340, https://doi.org/ 10.5194/acp-16-13321-2016, 2016.
603 Feng, S., Zhang, L., Wang, S., Nadykto, A. B., Xu, Y., Shi, Q., Jiang, B., and Qian, W.:
604 Characterization of dissolved organic nitrogen in wet deposition from Lake Erhai basin by using
605 ultrahigh resolution FT-ICR mass spectrometry, Chemosphere, 156, 438-445,
606 https://doi.org/10.1016/j.chemosphere.2016.04.039, 2016.
607 Feng, Y., Ramanathan, V., and Kotamarthi, V. R.: Brown carbon: a significant atmospheric
608 absorber of solar radiation?, Atmos. Chem. Phys., 13, 8607-8621,
609 https://doi.org/10.5194/acp-13-8607-2013, 2013.
610 Fu, P., Kawamura, K., Chen, J., Qin, M., Ren, L., Sun, Y., Wang, Z., Barrie, L. A., Tachibana, E.,
611 Ding, A., and Yamashita, Y.: Fluorescent water-soluble organic aerosols in the High Arctic
612 atmosphere, Sci Rep, 5, 9845, https://doi.org/10.1038/srep09845, 2015.
613 Gu, Q., and Kenny, J. E.: Improvement of Inner Filter Effect Correction Based on Determination
614 of Effective Geometric Parameters Using a Conventional Fluorimeter, Anal. Chem., 81,
615 420-426, https://doi.org/10.1021/ac801676j, 2009.
616 Jiang, B., Kuang, B. Y., Liang, Y., Zhang, J., Huang, X. H. H., Xu, C., Yu, J. Z., and Shi, Q.:
617 Molecular composition of urban organic aerosols on clear and hazy days in Beijing: a
618 comparative study using FT-ICR MS, Environ. Chem., 13, 888-901,
619 https://doi.org/10.1071/en15230, 2016.
620 Kahnt, A., Behrouzi, S., Vermeylen, R., Safi Shalamzari, M., Vercauteren, J., Roekens, E., Claeys,
621 M., and Maenhaut, W.: One-year study of nitro-organic compounds and their relation to wood
622 burning in PM10 aerosol from a rural site in Belgium, Atmos. Environ., 81, 561-568,
623 https://doi.org/10.1016/j.atmosenv.2013.09.041, 2013.
624 Kirchstetter, T. W., and Thatcher, T. L.: Contribution of organic carbon to wood smoke particulate
625 matter absorption of solar radiation, Atmos. Chem. Phys., 12, 5803-5816,
626 https://doi.org/10.5194/acp-12-6067-2012, 2012.
627 Laskin, A., Laskin, J., and Nizkorodov, S. A.: Chemistry of atmospheric brown carbon, Chem.
628 Rev., 115, 4335-4382, https://doi.org/10.1021/cr5006167, 2015.
629 Lee, H. J., Laskin, A., Laskin, J., and Nizkorodov, S. A.: Excitation-emission spectra and

https://doi.org/10.5194/acp-2019-584
Preprint. Discussion started: 7 August 2019

630 fluorescence quantum yields for fresh and aged biogenic secondary organic aerosols, Environ.
631 Sci. Technol., 47, 5763-5770, https://doi.org/10.1021/es400644c 2013.
632 Li, M., Fan, X., Zhu, M., Zou, C., Song, J., Wei, S., Jia, W., and Peng, P.: Abundances and light
633 absorption properties of brown carbon emitted from residential coal combustion in China,
634 Environ. Sci. Technol., 53, 595-603, https://doi.org/10.1021/acs.est.8b05630, 2018.
635 Lin, P., Yu, J. Z., Engling, G., and Kalberer, M.: Organosulfates in humic-like substance fraction
636 isolated from aerosols at seven locations in East Asia: a study by ultra-high-resolution mass
637 spectrometry, Environ. Sci. Technol., 46, 13118-13127, https://doi.org/10.1021/es303570v,
638 2012.
639 Lin, P., Aiona, P. K., Li, Y., Shiraiwa, M., Laskin, J., Nizkorodov, S. A., and Laskin, A.:
640 Molecular Characterization of Brown Carbon in Biomass Burning Aerosol Particles, Environ.
641 Sci. Technol., 50, 11815-11824, https://doi.org/10.1021/acs.est.6b03024, 2016.
642 Lin, P., Fleming, L. T., Nizkorodov, S. A., Laskin, J., and Laskin, A.: Comprehensive Molecular
643 Characterization of Atmospheric Brown Carbon by High Resolution Mass Spectrometry with
644 Electrospray and Atmospheric Pressure Photoionization, Anal. Chem., 90, 12493-12502,
645 https://doi.org/10.1021/acs.analchem.8b02177, 2018.
646 Luciani, X., Mounier, S., Redon, R., and Bois, A.: A simple correction method of inner filter
647 effects affecting FEEM and its application to the PARAFAC decomposition, Chemom. Intell.
648 Lab. Syst., 96, 227-238, https://doi.org/10.1016/j.chemolab.2009.02.008, 2009.
649 Matos, J. T. V., Freire, S. M. S. C., Duarte, R. M. B. O., and Duarte, A. C.: Natural organic matter
650 in urban aerosols: Comparison between water and alkaline soluble components using
651 excitation–emission matrix fluorescence spectroscopy and multiway data analysis, Atmos.
652 Environ., 102, 1-10, https://doi.org/10.1016/j.atmosenv.2014.11.042, 2015.
653 Mo, Y., Li, J., Liu, J., Zhong, G., Cheng, Z., Tian, C., Chen, Y., and Zhang, G.: The influence of
654 solvent and pH on determination of the light absorption properties of water-soluble brown
655 carbon, Atmos. Environ., 161, 90-98, https://doi.org/10.1016/j.atmosenv.2017.04.037, 2017.
656 Mo, Y., Li, J., Jiang, B., Su, T., Geng, X., Liu, J., Jiang, H., Shen, C., Ding, P., Zhong, G., Cheng,
657 Z., Liao, Y., Tian, C., Chen, Y., and Zhang, G.: Sources, compositions, and optical properties of
658 humic-like substances in Beijing during the 2014 APEC summit: Results from dual carbon
659 isotope and Fourier-transform ion cyclotron resonance mass spectrometry analyses, Environ.

https://doi.org/10.5194/acp-2019-584
Preprint. Discussion started: 7 August 2019

Atmospheric Chemistry and Physics Discussions

660 Pollut., 239, 322-331, https://doi.org/10.1016/j.envpol.2018.04.041, 2018.
661 Murphy, K. R., Butler, K. D., Spencer, R. G., Stedmon, C. A., Boehme, J. R., and Aiken, G. R.:
662 Measurement of dissolved organic matter fluorescence in aquatic environments: an
663 interlaboratory comparison, Environ. Sci. Technol., 44, 9405-9412,
664 https://doi.org/10.1021/es102362t, 2010.
665 Murphy, K. R., Stedmon, C. A., Graeber, D., and Bro, R.: Fluorescence spectroscopy and
666 multi-way techniques. PARAFAC, Anal. Methods, 5, 6557-6566,
667 https://doi.org/10.1039/c3ay41160e, 2013.
668 Park, S. S., and Yu, J.: Chemical and light absorption properties of humic-like substances from
669 biomass burning emissions under controlled combustion experiments, Atmos. Environ., 136,
670 114-122, https://doi.org/10.1016/j.atmosenv.2016.04.022, 2016.
671 Patriarca, C., Bergquist, J., Sjoberg, P. J. R., Tranvik, L., and Hawkes, J. A.: Online
672 HPLC-ESI-HRMS Method for the Analysis and Comparison of Different Dissolved Organic
673 Matter Samples, Environ. Sci. Technol., 52, 2091-2099, https://doi.org/10.1021/acs.est.7b04508,
674 2018.
675 Qin, J., Zhang, L., Zhou, X., Duan, J., Mu, S., Xiao, K., Hu, J., and Tan, J.: Fluorescence
676 fingerprinting properties for exploring water-soluble organic compounds in PM 2.5 in an
677 industrial city of northwest China, Atmos. Environ., 184, 203-211,
678 https://doi.org/10.1016/j.atmosenv.2018.04.049, 2018.
679 Riva, M., Tomaz, S., Cui, T. Q., Lin, Y. H., Perraudin, E., Gold, A., Stone, E. A., Villenave, E.,
680 and Surratt, J. D.: Evidence for an Unrecognized Secondary Anthropogenic Source of
681 Organosulfates and Sulfonates: Gas-Phase Oxidation of Polycyclic Aromatic Hydrocarbons in
682 the Presence of Sulfate Aerosol, Environ. Sci. Technol., 49, 6654-6664,
683 https://doi.org/10.1021/acs.est.5b00836, 2015.
684 Saleh, R., Robinson, E. S., Tkacik, D. S., Ahern, A. T., Liu, S., Aiken, A. C., Sullivan, R. C.,
685 Presto, A. A., Dubey, M. K., Yokelson, R. J., Donahue, N. M., and Robinson, A. L.: Brownness
686 of organics in aerosols from biomass burning linked to their black carbon content, Nat. Geosci.,
687 7, 647-650, https://doi.org/10.1038/ngeo2220, 2014.
688 Sgroi, M., Roccaro, P., Korshin, G. V., and Vagliasindi, F. G. A.: Monitoring the Behavior of
689 Emerging Contaminants in Wastewater-Impacted Rivers Based on the Use of Fluorescence

https://doi.org/10.5194/acp-2019-584
Preprint. Discussion started: 7 August 2019

Atmospheric Chemistry and Physics Discussions

690 Excitation Emission Matrixes (EEM), Environ. Sci. Technol., 51, 4306-4316,
691 https://doi.org/10.1021/acs.est.6b05785, 2017.
692 Shimabuku, K. K., Kennedy, A. M., Mulhern, R. E., and Summers, R. S.: Evaluating Activated
693 Carbon Adsorption of Dissolved Organic Matter and Micropollutants Using Fluorescence
694 Spectroscopy, Environ. Sci. Technol., 51, 2676-2684, https://doi.org/10.1021/acs.est.6b04911,
695 2017.
696 Sleighter, R. L., Chen, H., Wozniak, A. S., Willoughby, A. S., Caricasole, P., and Hatcher, P. G.:
697 Establishing a measure of reproducibility of ultrahigh-resolution mass spectra for complex
698 mixtures of natural organic matter, Anal. Chem., 84, 9184-9191,
699 https://doi.org/10.1021/ac3018026, 2012.
700 Song, J., Li, M., Jiang, B., Wei, S., Fan, X., and Peng, P.: Molecular Characterization of
701 Water-Soluble Humic like Substances in Smoke Particles Emitted from Combustion of Biomass
702 Materials and Coal Using Ultrahigh-Resolution Electrospray Ionization Fourier Transform Ion
703 Cyclotron Resonance Mass Spectrometry, Environ. Sci. Technol., 52, 2575-2585,
704 https://doi.org/10.1021/acs.est.7b06126, 2018.
705 Sun, H., Biedermann, L., and Bond, T. C.: Color of brown carbon: A model for ultraviolet and
706 visible light absorption by organic carbon aerosol, Geophys. Res. Lett., 34,
707 https://doi.org/10.1029/2007gl029797, 2007.
708 Tian, J., Ni, H., Cao, J., Han, Y., Wang, Q., Wang, X., Chen, L. W. A., Chow, J. C., Watson, J. G.,
709 Wei, C., Sun, J., Zhang, T., and Huang, R.: Characteristics of carbonaceous particles from
710 residential coal combustion and agricultural biomass burning in China, Atmos. Pollut. Res., 8,
711 521-527, https://doi.org/10.1016/j.apr.2016.12.006, 2017.
712 Wells, M. J. M., Mullins, G. A., Bell, K. Y., Da Silva, A. K., and Navarrete, E. M.: Fluorescence
713 and Quenching Assessment (EEM-PARAFAC) of de Facto Potable Reuse in the Neuse River,
714 North Carolina, United States, Environ. Sci. Technol., 51, 13592-13602,
715 https://doi.org/10.1021/acs.est.7b03766, 2017.
716 Wong, J. P. S., Nenes, A., and Weber, R. J.: Changes in Light Absorptivity of Molecular Weight
717 Separated Brown Carbon Due to Photolytic Aging, Environ. Sci. Technol., 51, 8414-8421,
718 https://doi.org/10.1021/acs.est.7b01739, 2017.
719 Wu, G., Ram, K., Fu, P., Wang, W., Zhang, Y., Liu, X., Stone, E. A., Pradhan, B. B., Dangol, P.

https://doi.org/10.5194/acp-2019-584
Preprint. Discussion started: 7 August 2019

720 M., Panday, A. K., Wan, X., Bai, Z., Kang, S., Zhang, Q., and Cong, Z.: Water-Soluble Brown
721 Carbon in Atmospheric Aerosols from Godavari (Nepal), a Regional Representative of South
722 Asia, Environ. Sci. Technol., 53, 3471-3479, https://doi.org/10.1021/acs.est.9b00596, 2019.
723 Yan, C., Zheng, M., Sullivan, A. P., Bosch, C., Desyaterik, Y., Andersson, A., Li, X., Guo, X.,
724 Zhou, T., Gustafsson, Ö., and Collett, J. L.: Chemical characteristics and light-absorbing
725 property of water-soluble organic carbon in Beijing: Biomass burning contributions, Atmos.
726 Environ., 121, 4-12, https://doi.org/10.1016/j.atmosenv.2015.05.005, 2015.
727 Yan, G., and Kim, G.: Speciation and Sources of Brown Carbon in Precipitation at Seoul, Korea:
728 Insights from Excitation-Emission Matrix Spectroscopy and Carbon Isotopic Analysis, Environ.
729 Sc.i Technol., 51, 11580-11587, https://doi.org/10.1021/acs.est.7b02892, 2017.
730 Yu, H., Liang, H., Qu, F., Han, Z. S., Shao, S., Chang, H., and Li, G.: Impact of dataset diversity
731 on accuracy and sensitivity of parallel factor analysis model of dissolved organic matter
732 fluorescence excitation-emission matrix, Sci Rep, 5, 10207, https://doi.org/10.1038/srep10207,
733 2015.
734 Zhang, X., Lin, Y. H., Surratt, J. D., Zotter, P., Prevot, A. S. H., and Weber, R. J.: Light ‐
735 absorbing soluble organic aerosol in Los Angeles and Atlanta: A contrast in secondary organic
736 aerosol, Geophys. Res. Lett., 38, https://doi.org/10.1029/2011GL049385, 2011.
737 Zhang, X., Lin, Y. H., Surratt, J. D., and Weber, R. J.: Sources, composition and absorption
738 Angstrom exponent of light-absorbing organic components in aerosol extracts from the Los
739 Angeles Basin, Environ. Sci. Technol., 47, 3685-3693, https://doi.org/10.1021/es305047b,
740 2013.
741 Zhao, Y., Hallar, A. G., and Mazzoleni, L. R.: Atmospheric organic matter in clouds: exact masses
742 and molecular formula identification using ultrahigh-resolution FT-ICR mass spectrometry,
743 Atmos. Chem. Phys., 13, 12343-12362, https://doi.org/10.5194/acp-13-12343-2013, 2013.
744 Zhu, C. S., Cao, J. J., Huang, R. J., Shen, Z. X., Wang, Q. Y., and Zhang, N. N.: Light absorption
745 properties of brown carbon over the southeastern Tibetan Plateau, Sci. Total Environ., 625,
746 246-251, https://doi.org/10.1016/j.scitotenv.2017.12.183, 2018.
747